Supplementary Information for
Measurement-induced state transitions in a superconducting qubit: beyond the rotating wave approximation

Daniel Sank,[1, *] Zijun Chen,[2, *] Mostafa Khezri,[3, 4, *] J. Kelly,[1] R. Barends,[1] B. Campbell,[2] Y. Chen,[1] B. Chiaro,[2] A. Dunsworth,[2] A. Fowler,[1] E. Jeffrey,[1] E. Lucero,[1] A. Megrant,[1] J. Mutus,[1] M. Neeley,[1] C. Neill,[2] P. J. J. O'Malley,[2] C. Quintana,[2] P. Roushan,[1] A. Vainsencher,[1] T. White,[1] J. Wenner,[2] Alexander N. Korotkov,[3] and John M. Martinis[1, 2]

[1]*Google Inc., Santa Barbara, California 93117, USA*
[2]*Department of Physics, University of California, Santa Barbara, California 93106-9530, USA*
[3]*Department of Electrical and Computer Engineering, University of California, Riverside, California 92521, USA*
[4]*Department of Physics, University of California, Riverside, California 92521, USA*

HAMILTONIAN

The Hamiltonian of the coupled qubit-resonator system can be written as

$$H = H_{\mathrm{b}} + H_{\mathrm{I}} \tag{1}$$

where H_{b} is the "bare" Hamiltonian of the qubit and resonator, while H_{I} describes their capacitive coupling. With the ket convention $|\text{qubit, resonator}\rangle$, the bare Hamiltonian has the form

$$H_{\mathrm{b}} = \sum_{k,n} \left(E_k + n\hbar\omega_r \right) |k,n\rangle\langle k,n| \tag{2}$$

where ω_r is the (bare) resonator frequency, and E_k is the transmon energy of level k, calculated numerically using Mathieu characteristic functions [1]. The transmon transition frequencies are $\omega_{kl} \equiv (E_k - E_l)/\hbar$ and its anharmonicity is $\eta \equiv \omega_{21} - \omega_{10}$. This bare Hamiltonian produces the Jaynes-Cummings (JC) ladder of energy levels, shown in Fig. 3 in the main text.

The interaction Hamiltonian H_{I}, given by Eq. (2) in the main text, is due to charge-charge coupling between the resonator and transmon. It can be divided into two parts,

$$H_{\mathrm{I}} = H_{\mathrm{RWA}} + H_{\text{non-RWA}} , \tag{3}$$

where H_{RWA} contains only terms conserving total excitation number, while $H_{\text{non-RWA}}$ contains the rest of the terms. H_{RWA} has the form

$$H_{\mathrm{RWA}} = \sum_{k,n} \hbar g_{k,k+1}\sqrt{n} \, |k+1, n-1\rangle\langle k,n| + \mathrm{H.c.} , \tag{4}$$

where $g_{k,k'} \equiv g\langle k|Q|k'\rangle/\langle 0|Q|1\rangle$ are the normalized matrix elements of the transmon charge operator Q. These matrix elements are calculated numerically using Mathieu functions. In the case $k' = k+1$, the matrix elements are approximately (for not very large values of k)

$$g_{k,k+1} \approx g\sqrt{k+1} \left(1 + \frac{\eta}{2\omega_{10}} k \right) . \tag{5}$$
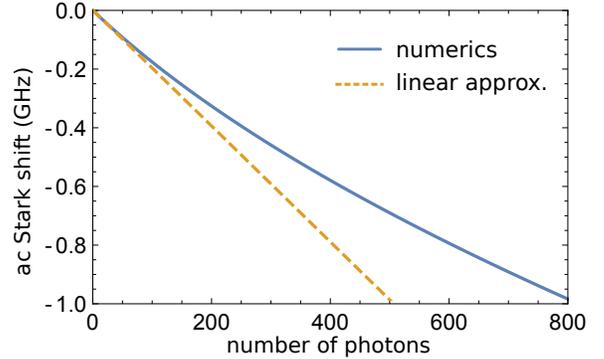
FIG. 1. Ac Stark shift of the transmon frequency as a function of the number of resonator photons n, for parameters of Fig. 2 in the main text ($n_c \approx 60$), using H_{RWA}. The solid line shows the value computed numerically, and the dashed line shows the conventional linear approximation $\delta\omega_{10} = -2|\chi|n$. As n becomes large, the relation between ac Stark shift and photon number becomes somewhat nonlinear.

By diagonalizing $H_{\mathrm{b}} + H_{\mathrm{RWA}}$, we find the eigenstates $\overline{|k,n\rangle}$ and eigenenergies $E_{\overline{|k,n\rangle}}$, which we use to numerically compute the frequencies $\overline{\omega}_k(n) = E_{\overline{|k,n-k\rangle}}/\hbar - n\omega_r$ within each RWA strip (see the fan energy diagram in Fig. 4a in the main text).

From $H_{\mathrm{b}} + H_{\mathrm{RWA}}$ we also numerically compute the photon number dependent ac Stark shift $\delta\omega_{10} \equiv \left(E_{\overline{|1,n\rangle}} - E_{\overline{|0,n\rangle}} \right)/\hbar - \omega_{10}$, as illustrated in Fig. 1. This map between resonator photon number and transmon ac Stark shift, which provides the calibration between drive power and photon number discussed in the main text, was the critical link between theory and experiment. Notice that Eq. (4) goes beyond the usual dispersive approximation [2]. In particular, the numerically computed curve deviates noticeably from the usual linear relation $\delta\omega_{10} = -2|\chi|n$.

The rest of the charge-charge interaction terms do not preserve excitation number, and are called here "non-RWA" terms. Although some of these terms are as large as RWA terms, they are usually neglected since they

are more off-resonant than RWA terms. However, these terms connect RWA strips and therefore enable resonant transitions in the JC ladder, as explained in the main text. In general, there are many types of non-RWA terms, which differ in coupling strength and in how close they are to resonantly connecting two JC ladder levels. We only consider terms involving $g_{k,k+1}$ and $g_{k,k+3}$, as they are the largest and least off-resonant,

$$
\begin{aligned}
H_{\text{non-RWA}}^{(1)} = &\sum_{k,n} \hbar\, g_{k,k+1} \sqrt{n+1}\, |k+1, n+1\rangle\langle k, n| + \text{H.c.} \\
&+ \sum_{k,n} \hbar\, g_{k,k+3} \sqrt{n}\, |k+3, n-1\rangle\langle k, n| + \text{H.c.}.
\end{aligned}
\tag{6}
$$

The couplings $g_{k,k+3}$ are calculated numerically; they are much smaller than $g_{k,k+1}$, as seen from the approximate formula

$$
g_{k,k+3} \approx g\sqrt{(k+1)(k+2)(k+3)}\, \frac{-\eta}{4\omega_{10}}.
\tag{7}
$$

In spite of being relatively small, these couplings are numerically more important in our problem than couplings $g_{k,k+1}$. We note that $H_{\text{non-RWA}}$ induces slight changes in the eigenenergies $E_{\overline{|k,n\rangle}}$, but the effect is small enough that we neglect it.

Equation (6) does not have any terms of the form $g_{k,k+2}$, and therefore only connects RWA strips differing in total excitation number by 2, which we call "next-nearest neighbors" (see Fig. 3 in the main text). The absence of $g_{k,k+2}$ terms is due to the symmetry of the transmon potential (in the phase basis). However, the real system violates this selection rule (see Fig. 2b discussed later and also the discussion in the main text). Accounting for the broken symmetry adds terms to $H_{\text{non-RWA}}$,

$$
H_{\text{non-RWA}}^{(2)} = \sum_{k,n} \hbar\, g_{k,k+2} \sqrt{n}\, |k+2, n-1\rangle\langle k, n| + \text{H.c.}.
\tag{8}
$$

The non-RWA terms of Eq. (8) connect RWA strips differing in total excitation number by 1, which we call "nearest neighbors" (see Fig. 3 in the main text), leading to additional resonance processes, such as $\overline{|0,n\rangle} \to \overline{|3, n-2\rangle}$.

EFFECTIVE COUPLING

When a resonance occurs between the initial state $\overline{|0,n\rangle}$ and, e.g., $\overline{|6, n-4\rangle}$, the system can make a resonant transition. In the perturbative language, in making this transition the system goes through several intermediate off-resonant states (see Fig. 3 in the main text); many different paths are available (i.e. different virtual processes). As an example, one path is $|0,n\rangle \to |1, n-1\rangle \to |4, n-2\rangle \to |5, n-3\rangle \to |6, n-4\rangle$, which involves the matrix element $g_{1,4}$. The condition of

resonance is necessary but not sufficient to give these processes a measurably large probability; the process must also have large enough effective coupling between initial and final states. We define the effective coherent coupling $g_{\text{eff}}^{\text{coh}}$ as

$$
g_{\text{eff}}^{\text{coh}} = \overline{\langle k_f, n_f|} H_{\text{non-RWA}} \overline{|k_i, n_i\rangle},
\tag{9}
$$

where $\overline{|k_i, n_i\rangle}$ and $\overline{|k_f, n_f\rangle}$ are the initial and final eigenstates, respectively. To find $g_{\text{eff}}^{\text{coh}}$, we expand the (RWA) eigenstates in the bare state basis,

$$
\overline{|k,n\rangle} = \sum_{l=0}^{k_{\max}} c_l^{(k,n)} |l, n+k-l\rangle,
\tag{10}
$$

where $k_{\max} \simeq 9$ is the highest transmon level taken into account. This expansion is then substituted into Eq. (9). In particular, for the transition $\overline{|0,n\rangle} \to \overline{|k, n-k+2\rangle}$ (to the next-nearest neighboring RWA strip) the effective coupling is

$$
\begin{aligned}
g_{\text{eff}}^{\text{coh}} = &\sum_l c_l^{(0,n)} \hbar g_{l,l+1} \sqrt{n-l+1}\, \left[c_{l+1}^{(k,n-k+2)}\right]^* \\
&+ \sum_l c_l^{(0,n)} \hbar g_{l,l+3} \sqrt{n-l}\, \left[c_{l+3}^{(k,n-k+2)}\right]^*.
\end{aligned}
\tag{11}
$$

Each term in Eq. (11) corresponds to a particular path in the picture of virtual processes. The paths in the first line are $|0,n\rangle \to |l, n-l\rangle \to |l+1, n-l+1\rangle \to |k, n-k+2\rangle$, where the first and last arrows describe subpaths within the RWA strips. Similarly, the terms in the second line correspond to paths $|0,n\rangle \to |l, n-l\rangle \to |l+3, n-l-1\rangle \to |k, n-k+2\rangle$.

The solid red line in Fig. 2a shows $g_{\text{eff}}^{\text{coh}}$ for the $\overline{|0,n\rangle} \to \overline{|6, n-4\rangle}$ transition (so that n corresponds to the resonance condition $E_{\overline{|0,n\rangle}} \approx E_{\overline{|6,n-4\rangle}}$), calculated using Eq. (9) or, equivalently, Eq. (11). Note that the terms in Eq. (11) are large at $n > n_c$ because $g_{l,l+1}\sqrt{n} \approx |\Delta|\sqrt{l+1}\sqrt{n/4n_c}$ (typically a few GHz) and the amplitudes c_l are significant for several states within the RWA strip. Nevertheless, the result for $g_{\text{eff}}^{\text{coh}}$ shown by the solid red line in Fig. 2a is smaller than even one such term. The reason is an almost perfect cancellation of the terms in Eq. (11), which happens because while the coefficients $c_l^{(k,n-k+2)}$ alternate in sign with changing l for $l < k$, the coefficients $c_l^{(0,n)}$ are all positive [3]. Therefore, the terms in Eq. (11) have alternating signs and efficiently cancel each other.

This cancellation is probably not so efficient in the real physical system. When the transmon is in an upper state, it is more sensitive to noise sources (such as charge noise) and therefore experiences increased dephasing. This and the relatively low coherence of the resonator ($1/\kappa_r \approx 37\,\text{ns}$) may suppress coherence between the different paths contributing to Eq. (11). While it is difficult to accurately calculate the effective coupling g_{eff}
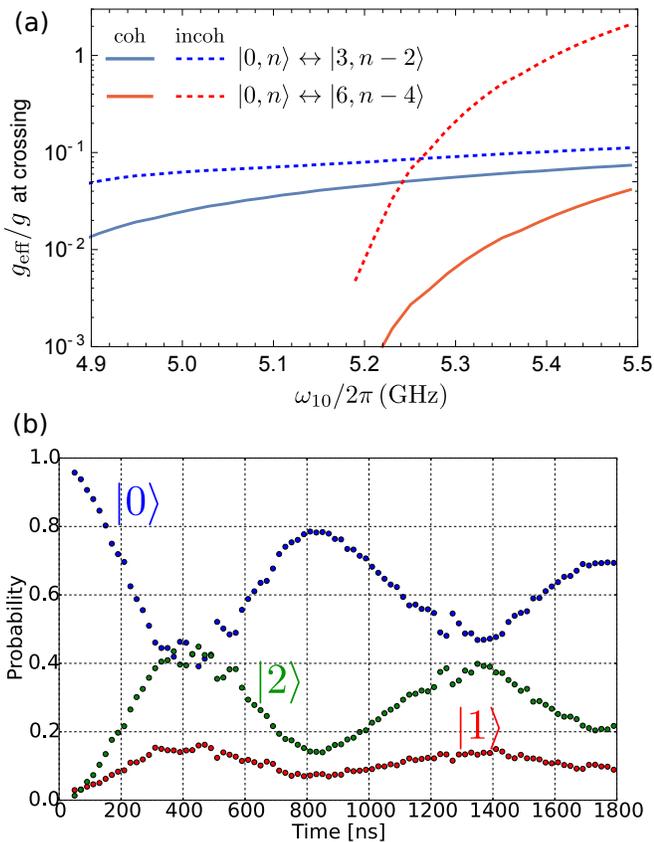
FIG. 2. (a) Effective coupling between crossing levels for different qubit frequencies. Solid and dashed lines show coherent and incoherent effective couplings respectively. The blue line assumes $g_{0,2}/g = 10^{-2}$. (b) Experimental observation of Rabi oscillation between transmon levels $|0\rangle$ and $|2\rangle$.

while accounting for decoherence, we can estimate the upper bound of the resulting g_{eff} as the fully incoherent sum of the terms in Eq. (11),

$$
\begin{aligned}
g_{\mathrm{eff}}^{\mathrm{incoh}} = \Bigg(& \sum_l \left| c_l^{(0,n)} \hbar g_{l,l+1} \sqrt{n-l+1} \left[c_{l+1}^{(k,n-k+2)} \right]^* \right|^2 \\
& + \sum_l \left| c_l^{(0,n)} \hbar g_{l,l+3} \sqrt{n-l} \left[c_{l+3}^{(k,n-k+2)} \right]^* \right|^2 \Bigg)^{1/2} .
\end{aligned}
$$
(12)

The red dashed line in Fig. 2a shows $g_{\mathrm{eff}}^{\mathrm{incoh}}$ for the $\overline{|0,n\rangle} \to \overline{|6,n-4\rangle}$ transition. We expect that the effective couplings in real system are between the results for fully coherent and fully incoherent cases (solid and dashed lines). The experimental feature B (which corresponds to the transition $\overline{|0,n\rangle} \to \overline{|6,n-4\rangle}$) can be well explained by effective coupling on the order of 1 MHz, which is in agreement with these theoretical values (note that $g/2\pi \approx 87\,\mathrm{MHz}$).

As discussed in the main text, the experimental feature A can be explained only if the state can transition between neighboring RWA strips (differing in total exci-

tation number by 1). However, if the transmon potential were exactly left/right symmetric, as is usually assumed, then $g_{k,k+2} = 0$, and this transition is forbidden. Therefore, to explain the feature A, we must assume that the transmon's symmetry is broken, leading to the additional non-RWA terms given in Eq. (8). We calculated the effective coupling at the $\overline{|0,n\rangle} \to \overline{|3,n-2\rangle}$ resonance, hypothesizing that $g_{k,k+2} = 0.01\,g\sqrt{(k+1)(k+2)}$ (i.e., 1% violation of the selection rule). The coupling for a coherent process is calculated via Eq. (9), which for the transitions $\overline{|0,n\rangle} \to \overline{|k,n-k+1\rangle}$ between the nearest-neighbor RWA strips produces

$$
g_{\mathrm{eff}}^{\mathrm{coh}} = \sum_l c_l^{(0,n)} \hbar g_{l,l+2} \sqrt{n-l} \left[c_{l+2}^{(k,n-k+1)} \right]^* .
$$
(13)

The numerical result, indicated by the solid blue line in Fig. 2a, shows that this 1% violation of the selection rule yields an effective coupling of a few MHz, which is large enough to explain the experimental feature A. The coupling becomes a few times larger if we assume the fully incoherent sum of the contributions from the paths in Eq. (13) (constructed similarly as Eq. (12))– see the dashed blue line in Fig. 2a. However, since the qubit state $|3\rangle$ is not supposed to experience a significant level of decoherence, we believe that the solid blue line is more relevant to the experimental situation than the dashed blue line. It is interesting to note that the difference between the dashed and solid blue lines is much smaller than between the dashed and solid red lines, indicating that the cancellation of terms in Eq. (13) is not as efficient as in Eq. (11). This is because for the transition $\overline{|0,n\rangle} \to \overline{|3,n-2\rangle}$ there are only two main terms in Eq. (13): those involving $g_{0,2}$ and $g_{1,3}$.

We experimentally looked for and actually observed the selection rule violation for $g_{0,2}$ by directly driving Rabi oscillations between transmon levels $|0\rangle$ and $|2\rangle$, as shown in Fig. 2b. By comparing the $|0\rangle \to |2\rangle$ Rabi oscillation period against the $|0\rangle \leftrightarrow |1\rangle$ Rabi oscillation period, and correcting for the differing microwave amplitude needed to drive those two transitions, we found experimentally that $g_{0,2}/g \simeq 10^{-2}$, surprisingly in good agreement with the guessed value. We emphasize that the experimental value of 10^{-2} should be considered only as an order of magnitude estimate.

We can offer only speculations about the possible physical mechanism behind the broken symmetry in the transmon. For example, it could result from SQUID asymmetry under external flux [4] or from a gradient of the magnetic field which couples to oscillating current in the circuit. However, these mechanisms are not investigated here and will be the subject of further studies.
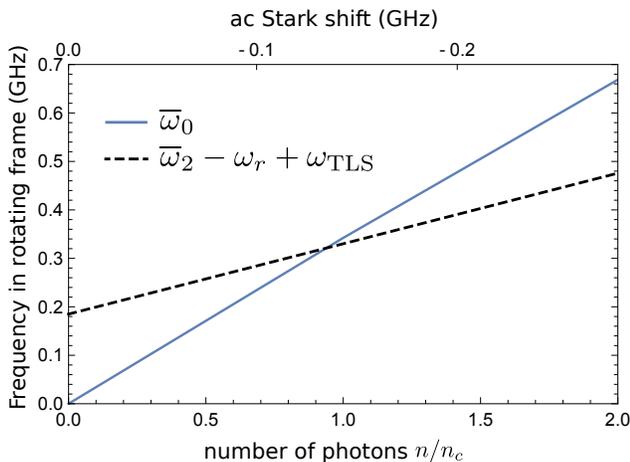
FIG. 3. Example of a resonance between transmon and a TLS. For a TLS with frequency 10 GHz, the level crossing occurs between $|0,n\rangle|0\rangle_{\mathrm{TLS}}$ and $|2,n-3\rangle|1\rangle_{\mathrm{TLS}}$.

TLS-ASSISTED TRANSITIONS

It is well known that microscopic defects in the materials comprising the transmon circuit can act as two level systems (TLS) and lead to qubit relaxation [5]. This relaxation can depend on the number of photons n in the resonator because of the ac Stark shift. Since ac Stark shift is approximately $\delta\omega_{10} = -2\,|\chi|\,n \simeq -(|\eta|\,/2)(n/n_c)$, the change of the qubit frequency is quite significant ($\sim \eta \approx -200\,\mathrm{MHz}$) when n is comparable to n_c. Therefore, even if the bare qubit frequency is chosen away from the TLS frequencies, it is possible that the qubit frequency will cross a TLS during measurement with a moderate value of n/n_c. In fact, we have experimentally observed this effect by comparing the transmon relaxation rate as a function of ω_{10} with $n = 0$ against that same relaxation rate during dispersive measurement. We found that the ac Stark shift induced by the resonator photons during dispersive measurement pushes the transmon into resonance with TLS's and therefore increases the relaxation rate (data not shown). Of course, increased relaxation degrades the fidelity of the quantum state measurement, so these crossings should be avoided.

Interestingly, coupling between the transmon and TLS's may also lead to transitions of the transmon to *higher* levels, similar to the effect of the non-RWA couplings associated with resonator. The level crossings associated with TLS's produce features similar to those produced by the non-RWA processes, such as dependence on Δ.

For example, the transmon can be excited from $|0\rangle$ to $|2\rangle$ via the following virtual process: $|0,n\rangle|0\rangle_{\mathrm{TLS}} \rightarrow |1,n-1\rangle|0\rangle_{\mathrm{TLS}} \rightarrow |2,n-2\rangle|0\rangle_{\mathrm{TLS}} \rightarrow |3,n-3\rangle|0\rangle_{\mathrm{TLS}} \rightarrow$

$|2,n-3\rangle|1\rangle_{\mathrm{TLS}}$. This process requires $\omega_{\mathrm{TLS}} \approx \omega_r + 2\,|\Delta| + |\eta|$ (the exact value is a little larger because of the level repulsion – see Fig. 3). The effective coupling for these resonances can be large enough to yield noticeable population transfer at lower photon numbers than for the non-RWA resonances. The example shown in Fig. 3 has a TLS with a frequency of 10 GHz and the resonance for the process described above occurs at $n/n_c \approx 1$. This value is sufficient for a noticeable amplitude of the bare state $|3, n-3\rangle$ ($c_3^{(0,n)} \approx 0.03$) and therefore a noticeable effective coupling for the process.

A TLS-assisted qubit transition from $|0\rangle$ to $|1\rangle$ requires only population of the bare state $|2, n-2\rangle$, and therefore the effective coupling becomes significant at values of n/n_c smaller than for the transition $|0\rangle \rightarrow |2\rangle$. For example, for the parameters, corresponding to the peak in the $|1\rangle$ probability (red line) in Fig. 2c of the main text ($n/n_c \approx 1.7$), the amplitude of the $|2\rangle$ component is quite significant, $c_2^{(0,n)} \approx 0.2$. Therefore, even a weak coupling between the transmon and a TLS with frequency $\omega_{\mathrm{TLS}}/2\pi \approx 8.4\,\mathrm{GHz}$ can explain this experimental peak. Note that when the TLS is sufficiently incoherent (e.g., because of fast energy relaxation), then the resonance condition could transform into a threshold-like condition, i.e., it should be enough energy to excite the TLS, also exciting the qubit, by transferring two photons from the resonator into the qubit-TLS system.

With increasing n/n_c and therefore increasing population of bare states $|k, n-k\rangle$, the number of possible TLS-assisted processes becomes larger (involving more final states), which increases the possibility of a transition away from the initial qubit state. We guess that the TLS-assisted processes may be responsible for the usual deterioration of qubit measurement fidelity in many experiments when increasing n becomes comparable to n_c (causing either excitation or relaxation of the transmon state).

---

[*] These authors contributed equally to this work

[1] J. Koch, T. M. Yu, J. Gambetta, A. A. Houck, D. I. Schuster, J. Majer, A. Blais, M. H. Devoret, S. M. Girvin, and R. J. Schoelkopf, Phys. Rev. A **76**, 042319 (2007).

[2] A. Blais, R.-S. Huang, A. Wallraff, S. M. Girvin, and R. J. Schoelkopf, Phys. Rev. A **69**, 062320 (2004).

[3] This follows from sequential perturbation theory with increasing energy compared to the initial energy $E_{|k,n-k+2\rangle}$.

[4] É. Dumur, B. Küng, A. Feofanov, T. Weißl, Y. Krupko, N. Roch, C. Naud, W. Guichard, and O. Buisson, IEEE Trans. Appl. Supercond. **26**, 1 (2016).

[5] J. M. Martinis, K. B. Cooper, R. McDermott, M. Steffen, M. Ansmann, K. D. Osborn, K. Cicak, S. Oh, D. P. Pappas, R. W. Simmonds, and C. C. Yu, Phys. Rev. Lett. **95**, 210503 (2005).